Redox Chemistry of Dimethylplatinum(II) Diimine Complexes. Oxidatively Induced Pt−Me Transfer between Transient Platinum(III) Cation Radicals

Lars Johansson,[1a] Olav B. Ryan,[1b] Christian Rømming,[1a] and Mats Tilset*,[1a,c]

Department of Chemistry, University of Oslo, P.O. Box 1033 Blindern, N-0315 Oslo, Norway, and SINTEF Applied Chemistry, Department of Hydrocarbon Process Chemistry, P.O. Box 124 Blindern, N-0314 Oslo, Norway

Received March 2, 1998

Downloaded by CARLI CONSORTIUM on June 30, 2009
Published on August 6, 1998 on http://pubs.acs.org | doi: 10.1021/om9801498

The redox chemistry of the series of Pt(II) diimine complexes L_2PtMe_2 (**1**; L_2 = Ar−N=CRCR=N−Ar, where Ar/R = 4-MeC_6H_4/H (**a**), 4-$MeOC_6H_4$/H (**b**), 4-MeC_6H_4/Me (**c**), 4-$MeOC_6H_4$/Me (**d**)), with particular emphasis on the oxidation processes, has been studied in detail. As seen by cyclic voltammetry, **1a**−**d** undergo two successive, reversible one-electron reductions at the diimine ligands and an irreversible, metal-centered one-electron oxidation. The oxidation of **1b** has been investigated in some detail. Chemical oxidation of **1b** with $Cp_2Fe^+PF_6^-$ in acetonitrile yields a near 1:1 ratio of the corresponding Pt(II) and Pt(IV) cations $L_2Pt(NCMe)Me^+$ (**2b**) and *fac*-$L_2Pt(NCMe)Me_3^+$ (**3b**). Controlled-potential electrolysis of **1b** yields mixtures of **2b** and **3b** in a 1:1 ratio, as well as the cis,cis (**4b**) and one cis,trans (**5b**) isomer of the dicationic Pt(IV) complexes $L_2Pt(NCMe)_2Me_2^{2+}$. The percentage of the dications **4b** and **5b** depended on the electrode potential. A mechanism involving methyl group transfer between two transient Pt(III) intermediates $L_2PtMe_2^{\bullet+}$ is proposed to account for the generation of **2b** and **3b**, whereas further oxidation of the Pt(III) species at the electrode eventually provides **4b** and **5b**. The X-ray crystal structures of **1b** and **3b**(OTf^-) have been determined. All Pt−Me bond distances in these two species are essentially identical, averaging 2.057(1) Å.

Introduction

Cationic, coordinately unsaturated transition-metal complexes are involved as highly reactive intermediates in important catalytic and stoichiometric reactions. For example, alkene polymerization is catalyzed by cationic, highly electrophilic catalysts derived from group 4 d^0 metallocene[2] as well as group 10 d^8 square-planar[3] catalyst precursors. The selective ethene/CO copolymerization is accomplished with similar cationic species derived from square-planar d^8 precatalysts.[4] Recently, alkane C−H bond activation has been achieved at cationic 16-electron Ir(III)[5] and 14-electron Pt(II)[6] metal centers. The reactive cationic species are commonly generated by electrophilic abstraction of anionic ligands (halide, alkyl, hydride) from suitable neutral precursors. Interestingly, it has been less commonly demonstrated that one-electron oxidation processes can also generate unsaturated cationic metal centers for early[7,8] (d^0) as well as late[9] (d^{10}) metals.

The one-electron oxidation of closed-shell dialkylmetal and hydridoalkylmetal complexes can induce homolytic (eq 1) or apparently concerted (eq 2) reductive elimination reactions. We have reported for some thoroughly

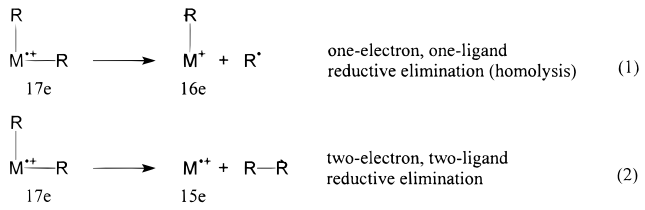

explored cases that the kinetics for the concerted-type reaction suggest that solvent coordination does not take place prior to or during the rate-limiting reductive elimination.[10,11] Consequently, these reactions appear to generate transient 15-electron species (eq 2) as the initially formed products. In the coordinating solvent

(1) (a) University of Oslo. (b) SINTEF. (c) E-mail: mats.tilset@kjemi.uio.no.
(2) (a) Bochmann, M. *J. Chem. Soc., Dalton Trans.* **1996**, 255. (b) Brintzinger, H. H.; Fischer, D.; Mülhaupt, R.; Rieger, B.; Waymouth, R. M. *Angew. Chem., Int. Ed. Engl.* **1995**, *34*, 1143.
(3) Johnson, L. K.; Killian, C. M.; Brookhart, M. *J. Am. Chem. Soc.* **1995**, *117*, 6414.
(4) Drent, E.; Budzelaar, P. H. M. *Chem. Rev.* **1996**, *96*, 663.
(5) Arndtsen, B. A.; Bergman, R. G. *Science* **1996**, *270*, 1970.
(6) Holtcamp, M. W.; Labinger, J. A.; Bercaw, J. E. *J. Am. Chem. Soc.* **1997**, *119*, 848.
(7) Jordan, R. F.; LaPointe, R. E.; Bajgur, C. S.; Echols, S. F.; Willett, R. *J. Am. Chem. Soc.* **1987**, *109*, 4111.
(8) Burk, M. J.; Tumas, W.; Ward, M. D.; Wheeler, D. R. *J. Am. Chem. Soc.* **1990**, *112*, 6133.
(9) Seligson, A. L.; Trogler, W. C. *J. Am. Chem. Soc.* **1992**, *114*, 7085.
(10) Pedersen, A.; Tilset, M. *Organometallics* **1993**, *12*, 56.
(11) Fooladi, E.; Tilset, M. *Inorg. Chem.* **1997**, *36*, 6021.

S0276-7333(98)00149-6 CCC: $15.00 © 1998 American Chemical Society
Publication on Web 08/06/1998

Scheme 1

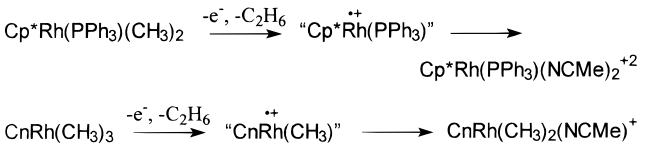

acetonitrile, these are subsequently transformed to the observed closed-shell products through additional oxidation, ligand coordination, or ligand redistribution processes, as shown by the examples[10,11] in Scheme 1.[12]

A plethora of square-planar Pd(II) and Pt(II) dialkyl complexes have been reported and vigorously studied, and the reduction chemistry of complexes with diimine and bipyridine or related ligands has been particularly well explored.[13] In contrast to this situation, their electron-transfer oxidation chemistry has not been investigated in much detail, perhaps due to the commonly observed irreversible electrode processes. The one-electron oxidation of the dialkyl compounds (dmpe)-$PdMe_2$ and (dmpe)$Pd(CH_2SiMe_3)_2$[9] was reported to induce the homolytic cleavage of a Pd−C bond to produce the cationic Pd(II) species (dmpe)Pd(R)(NC-Me)$^+$. Chen and Kochi[14] reported that the two-electron oxidation of *cis*-L_2PtR_2 (R = Me, Et; L = PPh_3, PMe_2-Ph) with $IrCl_6^{2-}$ in acetonitrile proceeded to give as Pt-containing products the Pt(II) complexes $L_2Pt(R)(X)$ (X = Cl, MeCN$^+$), resulting from single Pt−R homolysis (for R = Et and in part for Me), and two-electron-oxidized Pt(IV) products $L_2PtR_2X_2$ (for R = Me). Oxidation of the platinacyclobutane (bpy)$Pt(CH_2CH_2CH_2)$ was reported not to yield any C_2 or C_3 hydrocarbon gases; the fate of the Pt center of this complex and of $(PPh_3)_2$-$Pt(CH_2CH_2CH_2)$ after oxidation remains unclear.[15] Irreversible oxidative behavior of closely related Pt(II) bis(hydrocarbyl) species with bidentate, nitrogen-based chelating ligands such as substituted bipyridines or diimines has been frequently noted,[13,16−18] but the products of these oxidations have not yet been reported. Interestingly, some (diimine)Pt dimesityl complexes are reported to undergo reversible, metal-based oxidations to give Pt(III) cation radicals.[13,19−22] This enhanced stability has been attributed to steric shielding against axially directed nucleophilic attack, by solvent or other species, at the incipient Pt(III) cations. These species have, however, not been stable enough to be isolated nor have their decomposition products been identified.

We therefore wanted to explore the oxidation chemistry of these species in more detail. In this paper, we give an account of the synthesis, characterization, and redox chemistry of a series of (diimine)$PtMe_2$ complexes. In particular, we describe for the first time the products of the oxidatively induced reactions of the (diimine)-$PtMe_2$ complexes and show that they do not arise from concerted reductive elimination reactions or homolytic processes analogous to those described above. Rather, the predominant reaction pathway is a methyl group transfer from a transient Pt(III) intermediate, ultimately producing Pt(II) and Pt(IV) cationic products.

Scheme 2

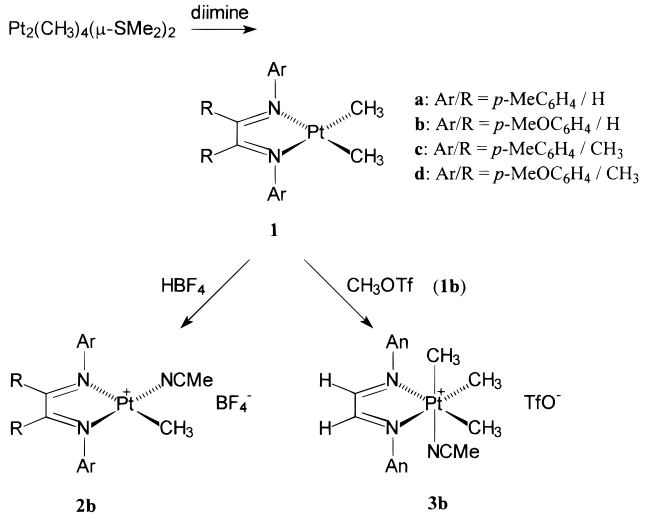

Results and Discussion

Synthesis and Characterization of (diimine)-$PtMe_2$ Complexes. Most of the complexes reported in this paper are new, and the details of their synthesis and characterization will be briefly given here. The dimethylplatinum(II) complexes L_2PtMe_2 (**1a**−**d**) were conveniently prepared (Scheme 2) in high yields from $Pt_2Me_4(\mu\text{-}SMe_2)_2$[23,24] and the appropriate diimine ligand L_2[12] (L_2 = ArN=CRCR=NAr; Ar/R = Tol/H (**a**; (previously reported[13,24]); An/H, **b**; Tol/Me, **c**; An/Me, **d**), adapting the procedures used by others for the preparation of related L_2PtMe_2 and (bpy)$PtMe_2$ complexes.[13,16,24−26] The compounds were characterized by ^{1}H and ^{13}C{^{1}H} NMR and UV−vis spectroscopy and by elemental analyses. A summary of key spectroscopic data for complexes prepared in this work is given in Table 1. The NMR spectra of **1a**−**d** clearly reflect their molecular symmetry. Satellites due to coupling to ^{195}Pt were observed in the ^{1}H NMR spectra for the Pt−Me groups ($^2J_{Pt-H}$ = ca. 87 Hz) as well as for the chelate ring C−H resonance in **1a**,**b**. The absorptions of the intensely colored compounds in their electronic spectra at λ ca. 500−600 nm are assigned to metal-to-ligand, d(Pt) → π^*(diimine), charge-transfer absorptions, in analogy with what has been established for related (diimine)Pt and (bpy)Pt complexes.[13] The MLCT absorptions exhibit the expected[13,17] solvent dependence

(12) Abbreviations: Cp* = (η^5-C_5Me_5); Cn = 1,4,7-trimethyl-1,4,7-triazacyclononane; dmpe = 1,4-bis(dimethylphosphino)ethane; Cy = cyclohexyl; Tol = *p*-tolyl; An = *p*-anisyl.

(13) Kaim, W.; Klein, A.; Hasenzahl, S.; Stoll, H.; Záliš, S.; Fiedler, J. *Organometallics* **1998**, *17*, 237 and references therein.
(14) Chen, J. Y.; Kochi, J. K. *J. Am. Chem. Soc.* **1977**, *99*, 1450.
(15) Klingler, R. J.; Huffman, J. C.; Kochi, J. K. *J. Am. Chem. Soc.* **1982**, *104*, 2147.
(16) Hasenzahl, S.; Hausen, H.-D.; Kaim, W. *Chem. Eur. J.* **1995**, *1*, 95.
(17) Braterman, P. S.; Song, J.-I.; Vogler, C.; Kaim, W. *Inorg. Chem.* **1992**, *31*, 222.
(18) Vogler, C.; Schwederski, B.; Klein, A.; Kaim, W. *J. Organomet. Chem.* **1992**, *436*, 367.
(19) Klein, A.; Kaim, W.; Waldhör, E.; Hausen, H.-D. *J. Chem. Soc., Perkin Trans. 2* **1995**, 2121.
(20) Klein, A.; Kaim, W.; Hornung, F. M.; Fiedler, J.; Zalis, S. *Inorg. Chim. Acta* **1997**, *264*, 269.
(21) Klein, A.; Hausen, H.-D.; Kaim, W. *J. Organomet. Chem.* **1992**, *440*, 207.
(22) Klein, A.; Kaim, W. *Organometallics* **1995**, *14*, 1176.
(23) Scott, J. D.; Puddephatt, R. J. *Organometallics* **1983**, *2*, 1643.
(24) van Asselt, R.; Rijnberg, E.; Elsevier, C. J. *Organometallics* **1994**, *13*, 706.
(25) Achar, S.; Scott, J. D.; Vittal, J. J.; Puddephatt, R. J. *Organometallics* **1993**, *12*, 4592.
(26) Monaghan, P. K.; Puddephatt, R. J. *Organometallics* **1984**, *3*, 444.

Downloaded by CARLI CONSORTIUM on June 30, 2009
Published on August 6, 1998 on http://pubs.acs.org | doi: 10.1021/om9801498

Table 1. Key Spectroscopic Data for New Complexes

	^{1}H NMR, δ^a			^{13}C{^{1}H} NMR,	UV−vis λ_{max}, nm ($10^{-3}\epsilon$, M^{-1} cm^{-1})	
compd	Pt−*Me* ($^2J(^{195}$Pt−H))	Pt−NC*Me* ($^4J(^{195}$Pt−H))	diimine *H*(*Me*) ($^3J(^{195}$Pt−H))	δ^a Pt−*Me* ($^2J(^{195}$Pt−H))	acetonitrile	toluene
1a	1.67 (87.9)		9.33 (29.1)	−11.4 (809)	377 (7.7), 550 sh (1.5), 595 (1.9)	397 (7.8), 600 sh (1.5), 651 (2.4)
1b	1.63 (87.8)		9.30 (28.7)	−11.5 (806)	394 (12.7), 560 sh (2.1), 595 (2.2)	411 (14.0), 605 (2.4), 649 (3.0)
1c	0.92 (86.9)		1.43	−13.5 (803)	372 (4.1), 510 sh (2.0), 541 (2.2)	453 (3.8), 595 (0.4)
1d	0.95 (86.6)		1.45	−13.5 (801)	369 (7.6), 510 sh (3.0), 543 (3.2)	378 (4.0), 550 (0.9), 597 (0.9)
2a	1.08 (76.6)	2.44 (13.9)	8.94 (99.8) 8.98 (35.6)	−10.8 (674)[b]	329 (6.9), 400 (9.9)	
2b	1.11 (76.5)	2.46 (14.0)	8.87 (97.9) 8.89 (33.6)	−10.7 (675)[b]	322 (5.0), 432 (13.2)	
2c	0.62 (75.1)	2.11 (13.6)	2.05 (10.2) 2.13	−11.9[d]	314 (4.8)	
2d	0.65 (75.1)	2.17 (13.6)	2.06 (10.3) 2.15	−11.7[d]	306 (4.4), 393 (5.1)	
3b	0.53 (76.3) (ax)[b] 0.94 (69.9) (eq)[b]	not obsd[b]	8.81 (26.6)[b]	−7.1 (ax)[b,d] −2.9 (eq)[b,d]	438 (12.4)	
4b[c]	1.59 (71.4)[b] 1.61 (61.2)[b]	2.61 (10.9)[b] 2.62 (12.4)[b]	8.75 (94.4)[b] 8.85 (30.4)[b]			
5b[c]	1.85 (62.7)[b]	2.66 (10.1)	9.05 (25.6)[b]			

[a] Dichloromethane-d_2 unless otherwise noted. [b] Acetonitrile-d_3. [c] Not isolated. Spectra of product mixture from exhaustive electrolysis. [d] Not resolved.

Downloaded by CARLI CONSORTIUM on June 30, 2009
Published on August 6, 1998 on http://pubs.acs.org | doi: 10.1021/om9801498

Table 2. Crystal Data and Structure Refinement for 1b and 3b(OTf$^-$)

	1b	**3b**(OTf$^-$)
empirical formula	$C_{18}H_{22}N_2O_2Pt$	$C_{22}H_{28}F_3N_3O_5PtS$
fw	493.47	698.62
temp, K	150(2)	150(2)
wavelength, Å	0.710 73	0.710 73
cryst syst	orthorhombic	triclinic
unit cell dimens[a]	a = 7.452(1)	a = 10.310(1) α = 99.47(1)
	b = 8.532(1)	b = 12.027(1) β = 113.60(1)
	c = 26.301(2)	c = 12.253(1) γ = 99.08(1)
V, Å^3; Z	1672.03(3); 4	1330.60(6); 4
density (ca.cd), Mg m^{-3}	1.960	1.744
abs coeff, mm^{-1}	8.403	5.408
F(000)	952	684
cryst size, mm	0.3 × 0.25 × 0.1	0.3 × 0.3 × 0.1
θ range for data, deg	2.51−40.68	1.77−28.73
no. of rflns collected	25 365	7746
no. of indep rflns	9530 (R(int) = 0.042)	5569 (R(int) = 0.050)
refinement method	full-matrix least squares on F^2	
no. of data/params	9526/210	5561/317
goodness of fit on F^2	1.095	1.053
final R indices	R1 = 0.040	R1 = 0.053
($I > 2\sigma(I)$)	wR2 = 0.086	wR2 = 0.122
R indices (all data)	R1 = 0.048	R1 = 0.068
	wR2 = 0.092	wR2 = 0.146
$\Delta\rho$(max), e Å^{-3}	5.33	3.32
$\Delta\rho$(min), e Å^{-3}	−3.65	−2.73

[a] a, b, c in Å; α, β, γ in deg.

Table 3. Selected Bond Lengths (Å) and Angles (deg) for 1b and 3b(OTf$^-$)

1b		**3b**(OTf$^-$)	
		Pt(1)−C(11)	2.053(8)
Pt(1)−C(9A)	2.061(4)	Pt(1)−C(9A)	2.060(8)
Pt(1)−C(9B)	2.046(5)	Pt(1)−C(9B)	2.066(8)
		Pt(1)−N(2)	2.160(6)
Pt(1)−N(1A)	2.138(4)	Pt(1)−N(1A)	2.187(7)
Pt(1)−N(1B)	2.113(4)	Pt(1)−N(1B)	2.194(7)
N(1A)−C(8A)	1.300(8)	N(1A)−C(8A)	1.297(10)
N(1A)−C(1A)	1.426(6)	N(1A)−C(1A)	1.458(9)
N(1B)−C(8B)	1.301(6)	N(1B)−C(8B)	1.289(11)
N(1B)−C(1B)	1.421(6)	N(1B)−C(1B)	1.441(9)
		N(2)−C(10)	1.132(10)
C(8A)−C(8B)	1.442(10)	C(8A)−C(8B)	1.470(11)
		C(10)−C(12)	1.457(11)
		C(11)−Pt(1)−C(9A)	89.6(3)
		C(11)−Pt(1)−C(9B)	88.3(3)
C(9A)−Pt(1)−C(9B)	85.6(2)	C(9A)−Pt(1)−C(9B)	84.6(3)
		C(11)−Pt(1)−N(2)	177.9(3)
		C(9A)−Pt(1)−N(2)	91.4(3)
		C(9B)−Pt(1)−N(2)	93.6(3)
		C(11)−Pt(1)−N(1A)	91.9(3)
C(9A)−Pt(1)−N(1A)	99.4(2)	C(9A)−Pt(1)−N(1A)	99.7(3)
C(9B)−Pt(1)−N(1A)	173.1(2)	C(9B)−Pt(1)−N(1A)	175.8(3)
		N(2)−Pt(1)−N(1A)	86.1(2)
		C(11)−Pt(1)−N(1B)	91.1(3)
C(9A)−Pt(1)−N(1B)	176.1(2)	C(9A)−Pt(1)−N(1B)	175.2(3)
C(9B)−Pt(1)−N(1B)	98.1(2)	C(9B)−Pt(1)−N(1B)	100.2(3)
		N(2)−Pt(1)−N(1B)	87.8(2)
N(1A)−Pt(1)−N(1B)	77.1(2)	N(1A)−Pt(1)−N(1B)	75.6(2)
C(8A)−N(1A)−C(1A)	116.4(5)	C(8A)−N(1A)−C(1A)	117.9(7)
C(8A)−N(1A)−Pt(1)	113.6(4)	C(8A)−N(1A)−Pt(1)	4.7(5)
C(1A)−N(1A)−Pt(1)	129.9(3)	C(1A)−N(1A)−Pt(1)	126.9(5)
C(8B)−N(1B)−C(1B)	117.1(4)	C(8B)−N(1B)−C(1B)	118.2(7)
C(8B)−N(1B)−Pt(1)	113.7(3)	C(8B)−N(1B)−Pt(1)	113.5(5)
C(1B)−N(1B)−Pt(1)	129.1(3)	C(1B)−N(1B)−Pt(1)	128.2(6)
		C(10)−N(2)−Pt(1)	169.8(7)
N(1A)−C(8A)−C(8B)	117.0(4)	N(1A)−C(8A)−C(8B)	116.8(8)
N(1B)−C(8B)−C(8A)	118.3(4)	N(1B)−C(8B)−C(8A)	119.3(7)
		N(2)−C(10)−C(12)	178.9(9)

with absorptions occurring at considerably shorter wavelengths for more polar solvents (acetonitrile vs toluene).

X-ray Crystallographic Structure Determination of 1b. Details about the structure determination for **1b** are given in the Experimental Section. Table 2 lists experimental and crystallographic data, and selected bond distances and angles for **1b** are given in Table 3. Figure 1 shows an ORTEP drawing of the X-ray crystal structure of **1b**. The molecule assumes the square-planar structure that is normally expected for a four-coordinate d^8 species. The average Pt−Me bond distance is 2.054 Å, and the Pt−N average is 2.126 Å. The chelate ring is planar, with a mean deviation from the least-squares plane of 0.026 Å. The planes of the arene rings A and B are rotated relative to the chelate ring plane by an average of 42.7° and are within 7.7° of being coplanar. The rotation of the aromatic rings out of planarity with the chelate is presumably caused by repulsions that would arise between the arene-ring ortho hydrogens and Pt−methyl and C(chelate)−hydrogen groups.

The main focus of the investigation was chosen to be on complex **1b**. The electrochemical and chemical oxidation (vide infra) of **1b** yielded mixtures of the four-coordinate Pt(II) species $L_2Pt(NCMe)Me^+$ (**2b**) and the

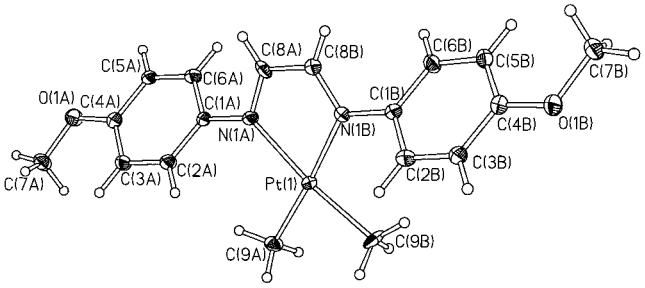

Figure 1. ORTEP plot of the structure of **1b**.

six-coordinate Pt(IV) species *fac*-$L_2Pt(NCMe)Me_3^+$ (**3b**) as the major products. These have been independently prepared and characterized.

Synthesis and Characterization of $L_2Pt(NCMe)Me^+$ (2a−d). When complexes **1a**−**d** were treated with a slight excess of $HBF_4{\cdot}Et_2O$ in acetonitrile, good yields of the complexes $L_2Pt(NCMe)Me^+BF_4^-$ (**2a**−**d**) were obtained. These salts have been characterized by their ^1H and $^{13}C\{^1H\}$ NMR spectra, UV−vis spectroscopy, and elemental analyses. Key spectroscopic data are given in Table 1. The ^1H NMR spectra are consistent with species of symmetry lower than the precursors **1a**−**d**, and separate signals are observed from the halves of the diimine ligands. The $^2J_{Pt-H}$ couplings to the Pt−Me groups are consistently somewhat smaller than for **1a**−**d** (ca 76 Hz vs 87 Hz). Couplings between Pt and coordinated *Me*CN were also seen; $^4J(^{195}Pt-H)$ = ca. 14 Hz.

The ^{195}Pt couplings to the C−H protons of the chelate ring were observed for **2a**,**b**. One such coupling was near 100 Hz and the other near 35 Hz. A complete assignment of the ^1H and ^{13}C NMR spectra of **2b** was carried out using a combination of H−H COSY, C−H COSY, and NOESY techniques. These spectra and details about the analysis are given in the Supporting Information; the results are summarized in Table 4. An inspection of the data shows that the signals assigned to atoms in the "left half" of the molecule (which includes the Pt−Me group), as drawn in Table 4, are slightly upfield relative to the corresponding signals of the "right half", except for the carbon resonances of the chelate ring and the arene ring ipso carbons. Simple considerations of relative trans effects of ligands are often used to rationalize trends in Pt−X couplings in square-planar complexes.[27] In **2b**, the $^3J_{Pt-H(d)}$ coupling (98 Hz) is greater than the $^3J_{Pt-H(e)}$ coupling (34 Hz). This is as might be anticipated since the methyl group, transoid relative to position (e), has a greater trans effect than the acetonitrile, which is transoid relative to position (d).

Synthesis and Characterization of *fac*-(AnN=CHCH=NAn)Pt(NCMe)$Me_3^+OTf^-$ (3b(OTf^-)). Treatment of **1b** with methyl triflate in acetonitrile at −13 °C produced **3b**(OTf^-) in high yield. The ^1H NMR spectrum of **3b** exhibits two Pt−Me signals in a 2:1 ratio with the diagnostic $^2J_{Pt-H}$ couplings, one signal due to coordinated acetonitrile, and one set of signals due to the diimine ligand. This is only consistent with a pseudo-octahedral structure in which the diimine ligand and two Pt−Me groups define an equatorial plane and the last Pt−Me and the acetonitrile ligand occupy the two apical positions, as shown in Scheme 2.

Table 4. ^1H and ^{13}C NMR Assignments for 2b[a]

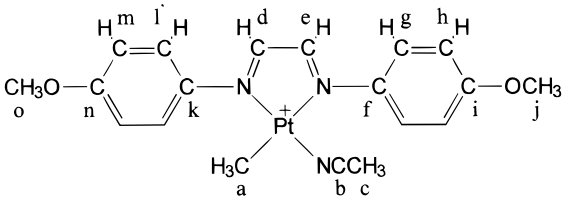

H or C atom	^1H NMR (dichloromethane-d_2)	^{13}C NMR (acetonitrile-d_3)
a	1.11 ($^2J_{Pt-H}$ = 76.5 Hz)	−10.7 ($^1J_{Pt-C}$ = 675 Hz)
b	n.a.	not obsd
c	2.46 ($^4J_{Pt-H}$ = 14.0 Hz)	not obsd
d	8.87 ($^3J_{Pt-H}$ = 97.9 Hz)	172.6
e	8.89 ($^3J_{Pt-H}$ = 33.6 Hz)	160.7 ($^2J_{Pt-C}$ = 57 Hz)
f	n.a.	140.9
g	7.56	125.9
h	7.10	115.9
i	n.a.	163.0
j	3.91	56.5
k	n.a.	141.4
l	7.27	125.6 ($^3J_{Pt-C}$ = 20 Hz)
m	7.01	115.0
n	n.a.	161.5
o	3.87	56.4

[a] Based on H−H COSY, C−H COSY, and NOESY spectra provided as Supporting Information.

The ^1H NMR spectrum of **3b** in acetonitrile-d_3 failed to show a signal due to the coordinated acetonitrile. However, a singlet due to free acetonitrile was clearly seen adjacent to the solvent signal, with correct integration. We attribute this to rapid exchange of initially coordinated acetonitrile and the solvent. In support of a rapid exchange process, we note that Elsevier and coworkers[24] have reported that a $L_2PtMe_3(NCMe)^+OTf^-$ complex in dichloromethane-d_2 solution exists as rapidly interconverting $[Pt]^+$-NCMe and [Pt−OTf] or five-coordinate $[Pt]^+(OTf^-)$ species ([Pt] = L_2PtMe_3). We have made similar observations that will be published elsewhere.

X-ray Crystallographic Structure Determination of *fac*-(AnN=CHCH=NAn)Pt(NCMe)$Me_3^+OTf^-$. Details about the structure determination for **3b**(OTf^-) are given in the Experimental Section. Table 2 lists experimental and crystallographic data, and Table 3 lists selected bond distances and angles. Figure 2 shows an ORTEP drawing of the X-ray crystal structure. The molecule adopts a pseudo-octahedral geometry. The apical and equatorial Pt−Me bond distances are statistically indistinguishable, averaging 2.060 Å, which is also essentially identical with the average Pt−Me distance of 2.053 Å in **1b**. The occurrence of identical apical and equatorial Pt−Me bond lengths in **3b** is in contrast to the situation for the Pt(IV) complex (CyN=CHCH=NCy)$PtMe_4$, in which the equatorial and apical Pt−Me distances were 2.045 and 2.140 Å, respectively.[16] The significantly greater apical Pt−Me distance in the latter case may be attributed to the greater trans effect of the Me ligand relative to MeCN. The chelate ring is planar, with a mean deviation from the least-squares plane of 0.020 Å. The planes of the arene rings A and

(27) Collman, J. P.; Hegedus, L. S.; Norton, J. R.; Finke, R. G. *Principles and Applications of Organotransition Metal Chemistry*; University Science Books: Mill Valley, CA, 1989; p 70.

Downloaded by CARLI CONSORTIUM on June 30, 2009
Published on August 6, 1998 on http://pubs.acs.org | doi: 10.1021/om9801498

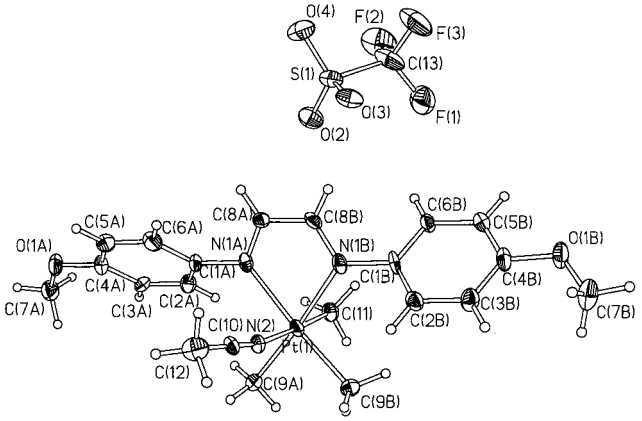

Figure 2. ORTEP plot of the structure of **3b**(OTf^-).

Table 5. Cyclic Voltammetry Data for (diimine)Pt Complexes[a]

compd	redn,[b] V vs Fc	oxidn,[c] V vs Fc
1a	−1.36, −2.11	0.6−0.7[c,e]
1b	−1.39, −2.15	0.6−0.7[c,e]
1c	−1.75, −2.55[c]	0.7[c,e]
1d	−1.76, −2.57[c]	0.7[c,e]
2a	−0.84, −1.65	
2b	−0.88, −1.70	
2c	−1.20, −1.92[d]	
2d	−1.21, −1.96[d]	
3b	−1.05, −1.74	

[a] Conditions: 1.0 mM substrate in acetonitrile/0.1 M Bu_4NPF_6, 20 °C, Pt-disk electrodes (d = 0.4 mm), v = 1.0 V/s. [b] Chemically reversible unless otherwise noted. [c] Peak potential for chemically irreversible couple. [d] Partially reversible couple. [e] Best response, as seen immediately after electrode polish. Great uncertainty due to adsorption problems.

B are rotated relative to the chelate ring plane by 48.9 and 50.5°, respectively, again presumably to relieve intramolecular repulsions. In contrast to the situation in **1b**, however, the A and B rings are mutually almost perpendicularly oriented (81.8°). The triflate anion is unexceptional, and the structure displays no unusual intermolecular contacts.

Cyclic Voltammetry Studies of (diimine)Pt Complexes. Transition-metal complexes containing bpy and diimine ligands typically undergo ligand-centered reductions to form reduced species that may be viewed as metal centers bonded to bpy or diimine anion radicals, as mentioned in the Introduction. In contrast, the consequences of the irreversible oxidation chemistry of (diimine)Pt dimethyl species remain poorly understood. We report in the following some interesting findings regarding the reductive and oxidative processes of these new species. Table 5 summarizes cyclic voltammetry data for most of the complexes that are reported in this paper.

Figure 3 shows cyclic voltammograms for the reduction and oxidation of **1b** (1.0 mM in acetonitrile/0.1 M $Bu_4N^+PF_6^-$, 20 °C, d = 0.4 mm Pt-disk electrode, voltage sweep rate v = 1.0 V/s). The complex undergoes two reversible reductions at −1.39 and −2.15 V vs the Cp_2Fe/Cp_2Fe^+ couple (Fc), with peak-to-peak separation of ca. 60 and 80−90 mV, respectively (the latter depending on electrode history), at v = 1.0 V/s. In comparison, the separation for Cp_2Fe was 60−62 mV under identical conditions. The reversible potentials $E°$, taken as the midpoints between the anodic and cathodic peaks, were

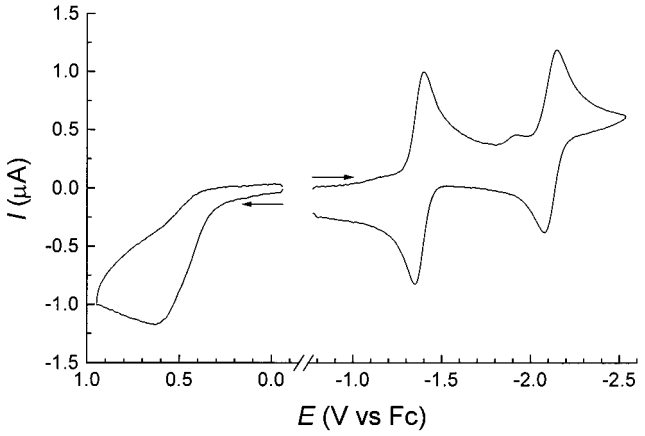

Figure 3. Cyclic voltammograms for the oxidation and reduction of (AnN=CHCH=NAn)$PtMe_2$ (**1b**). Conditions: 1.0 mM solution of **1b** in acetonitrile/0.1 M $Bu_4N^+PF_6^-$ at 20 °C (d = 0.4 mm Pt disk electrode, voltage sweep rate v = 1.0 V/s). The oxidative and reductive scans are done separately, with freshly conditioned electrode surface for each.

independent of the voltage sweep rate, and a plot of $I_p/v^{1/2}$ was linear. These data are in accord with two near-Nernstian one-electron-reduction processes. The oxidation of **1b** occurs irreversibly at ca. 0.7 V vs Fc. Adsorption problems caused the position of this irreversible peak to be quite variable. Peak potentials ranged between ca. 0.6 and 0.7 V at a freshly polished electrode and gradually underwent displacement to at least 1.0 V vs Fc after multiple repeated scans without intermittent electrode cleaning. Considerable signal broadening occurred at higher sweep rates, but it was evident that the oxidation was chemically irreversible even at v = 100 V/s, as evidenced by the lack of a cathodic peak during the reverse scan. This situation persisted when the voltammetry was performed in the poorly coordinating solvent dichloromethane. When the reductive scan after the oxidation of **1b** was taken to −2.4 V vs Fc, reduction peaks attributed to products from the follow-up reaction of $\mathbf{1b}^{\bullet+}$ were observed at ca −0.5 and −0.9 V. The peak at −0.5 V is assumed to arise from the reduction of a dicationic product of the oxidation (vide infra). The peak at −0.9 V closely matches the reduction peak for **2b** (vide infra), another oxidation product; a contribution from **3b** might be hidden under this peak due to the rather poor electrode behavior caused by the adsorption. These combined findings suggest that the observed Pt-containing products are formed on the CV time scale.

Each of the compounds **1a**,**c**,**d** also exhibited poorly reproducible, irreversible oxidation waves in acetonitrile.[28] However, whereas two reduction waves were also seen for **1b**−**d**, the behavior of **1c**,**d** differed from that of **1a**,**b** in that the last reduction process was chemically irreversible. When the reduction potential data for **1a**−**d** are compared, it is evident that the $E°$ values are very sensitive to the identity of the substituent at the carbon atoms of the chelate ring. The methyl-substituted complexes (**1c**,**d**) are more difficult to reduce than the unsubstituted ones (**1a**,**b**) by as much as 0.37−

(28) Kaim et al. have recently[13] reported that **1a** undergoes reversible reductions at −1.36 and −2.12 V and an irreversible oxidation at 0.65 V vs Fc. These data are in good agreement with ours.

Downloaded by CARLI CONSORTIUM on June 30, 2009
Published on August 6, 1998 on http://pubs.acs.org | doi: 10.1021/om9801498

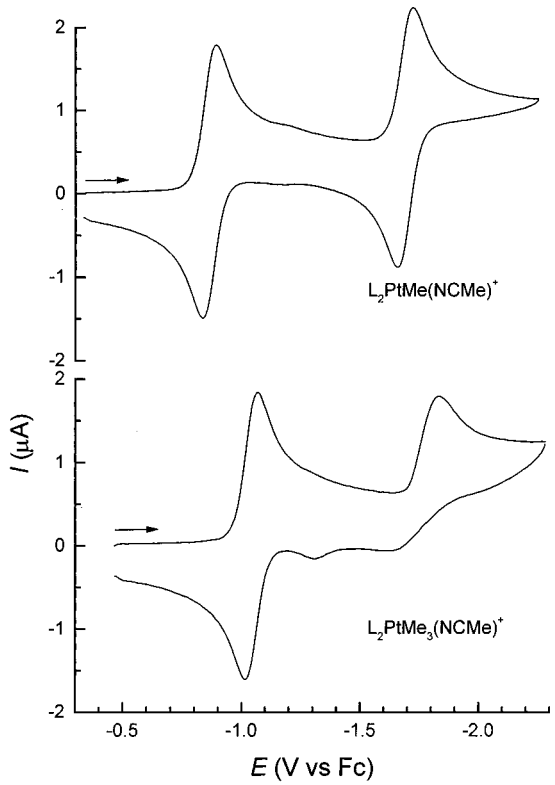

Figure 4. Cyclic voltammogram for the reduction of (AnN=CHCH=NAn)Pt(NCMe)$Me^+BF_4^-$ (**2b**(BF_4^-), bottom) and (AnN=CHCH=NAn)Pt(NCMe)$Me_3^+OTf^-$ (**3b**(OTf^-), top). Conditions as for the caption to Figure 3.

0.39 V. On the other hand, a change of the substituent at the aromatic ring has virtually no effect: the *p*-MeO-substituted species (**1b**,**d**) are more difficult to reduce than the *p*-Me-substituted species by only 0.03 V or less. This lack of sensitivity may be rationalized by the fact that the arene rings are twisted out of conjugation with the chelate ring, as found in the X-ray structure of **1b**. Thus, π interactions with the arene rings and their substituents are insignificant. Similar substituent effects have been previously observed for other metal complexes.[29]

Figure 4 shows cyclic voltammograms for the reduction of **2b**(BF_4^-) (bottom) and **3b**(OTf^-) (top). The cationic Pt(II) complex **2b** undergoes two reversible one-electron reduction processes at −0.88 and −1.70 V vs Fc. Both processes are presumed to be ligand-centered reductions. The first reduction occurs at a potential 0.51 V less negative than that for **1b**, which is also Pt(II). This difference reflects the fact that **2b** has a true positive charge, whereas **1b** does not. In comparison, the cationic Pt(IV) complex **3b** is reduced in a reversible wave at −1.05 V and an irreversible one at −1.74 V vs Fc. It is quite interesting to note that for the first reduction process, the *Pt(IV) complex is more difficult to reduce than the closely related Pt(II) complex!* Kaim and co-workers[13,16] noted that (CyN=CHCH=NCy)-$PtMe_2$ (Pt(II)) and (CyN=CHCH=NCy)$PtMe_4$ (Pt(IV)) exhibited essentially identical redox behavior as judged by CV experiments, for the reductive as well as for the oxidative processes, and the underlying electronic features were thoroughly analyzed. For complexes **2a**−**d**, it is again noteworthy that the chelate substituent has a great influence on the reduction potentials (0.33−0.36 V more difficult for Me vs H for the first reduction process), whereas the exchange of *p*-Me for *p*-MeO at the aryl rings has essentially no effect.

For the reduction of **3b**, a faint wave is seen on the reverse scan at ca. −1.25 V vs Fc. This wave was absent when the sweep was reversed after the *first* reduction. The faint wave therefore must arise from a product that is formed in the homogeneous reaction that follows after the second electron transfer. No attempts have been made at identifying the reduction product(s).

Electrochemical Bulk Oxidation of (AnN=CHCH=NAn)$PtMe_2$ (1b). Bulk oxidation of **1b** was performed under various conditions. The oxidations were performed at Pt- and Au-mesh electrodes and at each of the electrodes at working potentials of 0.85 and 0.95 V vs Fc. The location of these potentials in relation to the CV peak potential for **1b** cannot be exactly established, since the reproducibility of the CV oxidation peak potential was rather poor, and cyclic voltammograms at the large-mesh electrodes are rather ill-defined in any case. The charge that passed through the electrolysis cell was 1.1−1.6 faraday/mol, depending on the exact reaction conditions. Although trends extracted from the results of a limited number of experiments should be regarded with caution, the results suggest that a greater charge is consumed at the higher oxidation potential. The products of these electrolyses were analyzed by ^{1}H NMR spectroscopy. In all cases, **2b** and **3b** formed in a near 1:1 ratio (see Experimental Section for details). In addition, most notably when the higher electrode potential was used, dicationic species that have been tentatively identified as *cis*,*cis*-[(AnN=CHCH=NAn)$PtMe_2$(NCMe)$_2$]$^{2+}$ (**4b**) and *cis*,*trans*-[(AnN=CHCH=NAn)$PtMe_2$(NCMe)$_2$]$^{2+}$ (**5b**) were also produced. The spectroscopic data are given in the Experimental Section. The downfield chemical shifts (δ ca. 1.6) of the Pt−Me groups are consistent with a greater positive charge in these complexes than in **2b** and **3b**. Double sets of signals for all ligands were seen for **4b**; this is consistent only with the cis,cis formulation. For **5b**, single sets of signals are seen; this requires the presence of a mirror plane and could be consistent with structures in which the methyl groups are cis-disposed and occupy the equatorial plane while the acetonitrile ligands are trans-disposed in the apical positions, or vice versa. We have noticed that, in general, a $^3J_{Pt-H}$ coupling of the bridge hydrogens in the diimine ligand is observed to be relatively small in the cases where the hydrogens have a transoid Pt−*Me* group ($^3J_{Pt-H}$: **1a**, 29.1; **1b**, 28.7; **2a**, 35.6, **2b**, 33.6; **3b**, 26.6 Hz), whereas the corresponding value when the hydrogens have a transoid Pt-*NCMe* group are much greater (**2a**, 99.8; **2b**, 97.9; [(AnN=CHCH=NAn)Pt-(NCMe)$_2$]$^{2+}$, 97.7 Hz[30]). The *J* value for **5b**, 25.6 Hz, may therefore indicate that the methyl groups are located in the equatorial plane and the acetonitrile ligands in the apical positions, as suggested in Scheme 3.

(29) See for example: Rossenaar, B. D.; Hartl, F.; Stufkens, D. J. *Inorg. Chem.* **1996**, *35*, 6194.

(30) The dication can be straightforwardly prepared as its triflate salt by treatment of **1b** with 2 equiv of HOTf in dichloromethane, followed by addition of acetonitrile: Johansson, L.; Tilset, M. Unpublished work.

Downloaded by CARLI CONSORTIUM on June 30, 2009
Published on August 6, 1998 on http://pubs.acs.org | doi: 10.1021/om9801498

Scheme 3

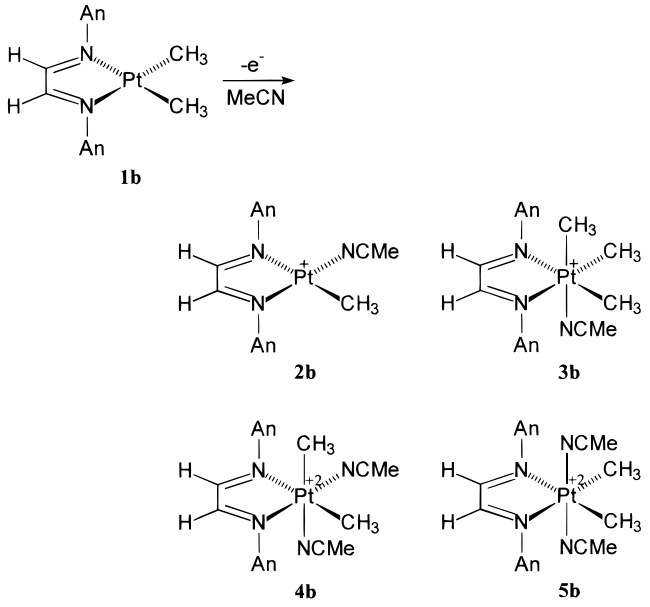

In those experiments where **4b** and **5b** were produced, **4b** was by far the dominant product of these two (**4b**:**5b** ratio of 3:1 or greater). Attempts at preparing these dicationic species by treatment of **2b** with methyl triflate were not successful; thus, their identification rests solely on the ^{1}H NMR data. A CV analysis of the electrolyte after a partial electrolysis oxidation at +0.95 V vs Fc showed, in addition to signals attributable to **2b** and **3b**, an intense reduction wave at −0.5 V. This value is ca. 0.5 V less negative than the reduction potentials for the monocationic products **2b** and **3b**, and therefore, we tentatively assign this wave to the reduction of one or both of the doubly charged species **4b** and **5b**.

Chemical Oxidation of (AnN=CHCH=NAn)PtMe$_2$ (1b). The oxidation of **1b** was effected with $Cp_2Fe^+PF_6^-$. The observed peak potential for the oxidation of **1b** (ca. +0.6 V vs Fc) dictates that the electron transfer from **1b** to Cp_2Fe^+ is highly endergonic; however, the rapid follow-up reaction caused the oxidation to take place relatively quickly in acetonitrile-d_3 at 55 °C. The ^{1}H NMR spectrum showed that a 56:44 mixture of **2b** and **3b** had been formed. Only small amounts of methane were discernible in the spectrum. The product composition was independent of the reaction temperature (55 °C vs slow heating from −25 °C to ambient over 4 days) as well as substrate concentration. Thus, chemical oxidation of **1b** leads to a near 1:1 mixture of **2b** and **3b**, in good agreement with the results of the electrochemical bulk oxidation.

Oxidation of 1b: Mechanistic Considerations. The combination of poor reproducibility and very fast follow-up homogeneous reaction causes the CV response for the oxidation of **1b** to be unsuitable for any detailed mechanistic analysis of the nature of this follow-up reaction. However, the product distribution under different reaction conditions allows an educated analysis of likely scenarios.

The essentially complete lack of methane or ethane in the homogeneous oxidation experiments rules out homolysis or reductive-elimination (eqs 1 and 2) processes as significant reaction pathways. Instead, bimolecular methyl transfer processes must be of major importance for these reactions, whether induced by chemical or electrochemical oxidation. Two scenarios are plausible for the bimolecular methyl transfer: a cation/cation **1b**$^{\bullet+}$/**1b**$^{\bullet+}$ reaction (Scheme 4), or a cation/neutral substrate **1b**$^{\bullet+}$/**1b** reaction (Scheme 5).

Scheme 4

$$L_2PtMe_2^{\bullet+} + L_2PtMe_2^{\bullet+} \longrightarrow L_2PtMe^+ + L_2PtMe_3^+$$

$$L_2PtMe^+ + MeCN \longrightarrow L_2PtMe(NCMe)^+$$

$$L_2PtMe_3^+ + MeCN \longrightarrow L_2PtMe_3(NCMe)^+$$

Scheme 5

$$L_2PtMe_2 + L_2PtMe_2^{\bullet+} \longrightarrow L_2PtMe^{\bullet} + L_2PtMe_3^+$$

$$L_2PtMe^{\bullet} + MeCN \longrightarrow L_2PtMe(NCMe)^{\bullet} \longrightarrow L_2PtMe(NCMe)^+ + e^-$$

$$L_2PtMe_3^+ + MeCN \longrightarrow L_2PtMe_3(NCMe)^+$$

The cation/cation reaction in Scheme 4 is attractive because it has been demonstrated, at least for closed-shell 18-electron complexes,[31] that one-electron oxidative processes lead to decreased M−X bond dissociation energies. Accordingly, Pt−Me cleavage should be more facile for $L_2PtMe_2^{\bullet+}$ than for L_2PtMe_2. According to Scheme 4, the two major cationic Pt(II) and Pt(IV) products will be formed in the observed 1:1 ratio observed for **2b** and **3b** after acetonitrile coordination at the immediate products of the methyl transfer.

Arguing against the first step in Scheme 4 is the fact that, at least under conditions of chemical oxidation with Cp_2Fe^+, the electron-transfer equilibrium concentration of $L_2PtMe_2^{\bullet+}$ will be very low (K_{eq} for the electron transfer is ca. 10^{-12} if $E_p = 0.7$ V vs Fc is taken as an approximate $E°$ value for the oxidation of L_2PtMe_2). This significantly reduces the likelihood that two such species will encounter each other to react, although it is not at all impossible within the constraints of diffusion control. As an alternative, in Scheme 5 we have indicated the transfer of a methyl radical from $L_2PtMe_2^{\bullet+}$ to L_2PtMe_2 or vice versa; coordination of acetonitrile at the resulting $L_2PtMe_3^+$ obviously gives the Pt(IV) product **3b**, whereas oxidation of the incipient $L_2PtMe^{\bullet}$ leads to the Pt(II) product **2b**. Oxidation of $L_2PtMe^{\bullet}$ may well occur via prior acetonitrile coordination. The radical that is produced by acetonitrile addition, $L_2PtMe(NCMe)^{\bullet}$, will be readily oxidized under the reaction conditions (its oxidation potential will be identical with the reduction potential for $L_2PtMe(NCMe)^+$ (**2b**; −0.88 V vs Fc).

Kaim and co-workers have suggested that the reactions of the Pt(III) intermediates $L_2PtR_2^{\bullet+}$ may involve axially directed attack by solvent or other nucleophiles,[13,17,21,22] although dimerization or aggregation phenomena were not discounted.[22] The indications for this were (1) solvent had a significant effect on the irreversible oxidation peak potentials for certain Pt(II) substrates and (2) dimesityl complexes $L_2Pt(mesityl)_2$, for which the approach of nucleophiles toward the axial positions is sterically blocked by the mesityl groups, exhibited reversible behavior by cyclic voltammetry. This possibility is fully consistent with our results: the acetonitrile solvent molecules may well coordinate at

(31) Tilset, M.; Hamon, J.-R.; Hamon, P. *Chem. Commun.*, in press.

Downloaded by CARLI CONSORTIUM on June 30, 2009
Published on August 6, 1998 on http://pubs.acs.org | doi: 10.1021/om9801498

Scheme 6

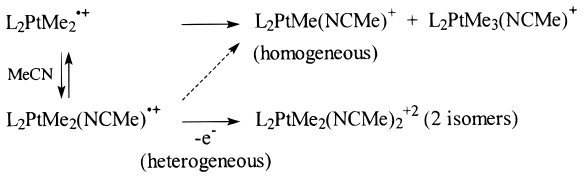

$L_2PtMe_2^{\bullet+}$ to give 17-electron pentacoordinate species $L_2PtMe_2(NCMe)^{\bullet+}$ *before* methyl transfer takes place according to Scheme 4 or 5, with the same options for the nature of the crucial methyl group transfer. Our finding that the oxidation of **1b** was chemically irreversible also in the poorly coordinating solvent dichloromethane may call for alternative explanations. For example, it is possible, and is consistent with experimental data available, that the "mesityl effect" is caused by a retardation of a *bimolecular* (Pt/Pt) reaction, as it could be impossible for two such sterically congested Pt centers to approach each other to within the distance required for the transfer of an organic ligand. The solvent effect on the oxidation peak potentials for the sterically less encumbered species may well be caused by changes in the heterogeneous electron-transfer rate constant, rather than by kinetic potential shifts caused by changes in the rates of the follow-up reactions.

We must next consider the results of the electrochemical oxidation reactions. It was established, at Pt as well as Au working electrodes, that the dicationic products **4b** and **5b** were favored when the working electrode potential was increased. Since the two dicationic products have retained both of the methyl groups that are present in the substrate, it is highly unlikely that their formation occurs via the one-electron oxidation products **2b** and **3b**. In support of this, the CV investigation also established that **2b** and **3b** showed no oxidation waves before the solvent/electrolyte discharge limit. Therefore, the formation of **4b** and **5b** must occur by interception of $\mathbf{1b}^{\bullet+}$ for further oxidation at the electrode surface before the methyl group is transferred. This explains why the yield of the dications is electrode potential dependent and, by extension, why no dications were produced by oxidation with the relatively mild oxidizing agent Cp_2Fe^+. (The oxidizing power of Cp_2Fe^+ is at least 0.8 V lower than the electrode potential employed for the electrolysis experiments.)

Scheme 6 summarizes the principal mechanistic features that have been discussed. The homogeneous reactions lead to the upper-right products, whereas the lower-right products arise from a secondary, heterogeneous electron-transfer reaction.

Conclusions

We have, for the first time, carried out a detailed study of the irreversible oxidation chemistry of (diimine)$PtMe_2$ complexes. Whereas previously investigated square-planar Pt(II) dialkyl complexes appear to[14,15] undergo Pt−R homolysis upon oxidation, the short-lived Pt(III) cation radicals $L_2PtMe_2^{\bullet+}$ studied by us appear to undergo intermolecular methyl transfer reactions to give the Pt(II) and Pt(IV) complexes $L_2Pt(NCMe)Me^+$ and *fac*-$L_2Pt(NCMe)Me_3^+$ as products. It is possible that the former is preceded by the 14-electron cation L_2PtMe^+, an analogue of the active species in C−H activation and alkene polymerization reactions. This opens the possibility that such catalysts may be generated by electron-transfer initiation.

Experimental Section

General Procedures. All manipulations involving organometallic compounds were carried out with use of vacuum line, Schlenk, syringe, or drybox techniques. Acetonitrile was distilled from P_2O_5, and acetonitrile-d_3, dichloromethane, and dichloromethane-d_2 were distilled from CaH_2. Acetonitrile and dichloromethane containing the supporting electrolyte were passed through a column of active neutral alumina prior to use to remove water and protic impurities before electrochemical measurements. The electrolyte was freed of air by purging with purified solvent-saturated argon, and all measurements and electrolyses were carried out under a blanket of argon.

^1H and $^{13}C\{^1H\}$ NMR spectra were recorded on Bruker Advance DXP 200, 300, and 500 instruments. Chemical shifts are reported in ppm relative to tetramethylsilane, with the residual solvent proton resonance as internal standard. Elemental analyses were performed by Ilse Beetz Mikroanalytisches Laboratorium, Kronach, Germany. UV−visible spectra were recorded on a Shimadzu UV-260 spectrophotometer and are reported as λ_{max} (nm) and $\epsilon \times 10^{-3}$ (M^{-1} cm^{-1}).

Electrochemical measurements were performed with an EG&G-PAR Model 273 potentiostat/galvanostat driven by an external HP 3314A sweep generator. The signals were fed to a Nicolet 310 digital oscilloscope and processed by an on-line personal computer. The working electrodes were Pt-disk electrodes (d = 0.4 mm), the counter electrode was a Pt wire, and the Ag-wire reference electrode assembly was filled with acetonitrile/0.01 M $AgNO_3$/0.1 M $Bu_4N^+PF_6^-$. The reference electrode was calibrated against Cp_2Fe, which was also used as the reference in this work. The positive-feedback *iR* compensation circuitry of the potentiostat was employed; the separation of anodic and cathodic peaks for the Cp_2Fe oxidation was 60−62 mV in acetonitrile.

$Pt_2Me_4(\mu\text{-}SMe_2)_2$[23] and the diimine ligands ArN=CHCH=NAr[32] and ArN=CMeCMe=NAr[33] were prepared according to reported methods.

General Procedure for the Preparation of Complexes (ArN=CRCR=NAr)$PtMe_2$ (1a−d). The diimine ligand ArN=CRCR=NAr was added to a solution of $Pt_2Me_4(\mu\text{-}SMe_2)_2$ in toluene. The solution was stirred at ambient temperature for 20 h. The solvent was removed, and the residue was recrystallized from a dichloromethane/pentane mixture. The product was obtained after drying in vacuo. For **1a**, this procedure resulted in a yield significantly improved over that reported recently (65%).[13]

(TolN=CHCH=NTol)$PtMe_2$ (1a): from $Pt_2Me_4(\mu\text{-}SMe_2)_2$ (600 mg, 1.044 mmol) and TolN=CHCH=NTol (494 mg, 2.090 mmol) in toluene (120 mL); dark green shimmering microcrystals (896 mg, 93%). ^1H NMR (300 MHz, dichloromethane-d_2): δ 1.67 (s, $^2J(^{195}Pt-H)$ = 87.9 Hz, 6 H, Pt*Me*), 2.42 (s, 6 H, Ar*Me*), 7.30 (m, 8 H, Ar *H*), 9.33 (s, $^3J(^{195}Pt-H)$ = 29.1 Hz, 2 H, NC*H*C*H*N). $^{13}C\{^1H\}$ NMR (75 MHz, dichloromethane-d_2): δ −11.4 ($^1J(^{195}Pt-C)$ = 809 Hz, Pt*Me*), 21.3 (Ar*Me*), 123.3 (Ar C_o), 129.8 (Ar C_m), 139.0 (Ar C_p), 147.8 ($^2J(^{195}Pt-C)$ = 28.5 Hz, Ar C_{ipso}), 161.6 (N*C*H*C*HN). UV−vis (acetonitrile): λ_{max} 377 (7.7), 550 sh (1.5), 595 (1.9). UV−vis (toluene): 397 (7.8), 600 sh (2.0), 651 (2.4). Anal. Calcd for $C_{18}H_{22}N_2Pt$: C, 46.85; H, 4.81; N, 6.07; Pt, 42.28. Found: C, 45.98; H, 4.54; N, 6.17; Pt, 42.05.

(AnN=CHCH=NAn)$PtMe_2$ (1b): from $Pt_2Me_4(\mu\text{-}SMe_2)_2$ (600 mg, 1.044 mmol) and AnN=CHCH=NAn (560 mg, 2.089 mmol) in toluene (120 mL); dark green shimmering micro-

(32) Kliegman, J. M.; Barnes, R. K. *J. Org. Chem.* **1970**, *35*, 3140.
(33) tom Dieck, H.; Svoboda, M.; Greiser, T. *Z. Naturforsch.* **1981**, *36B*, 823.

Downloaded by CARLI CONSORTIUM on June 30, 2009
Published on August 6, 1998 on http://pubs.acs.org | doi: 10.1021/om9801498

Downloaded by CARLI CONSORTIUM on June 30, 2009
Published on August 6, 1998 on http://pubs.acs.org | doi: 10.1021/om9801498

crystals (969 mg, 94%). ^{1}H NMR (300 MHz, dichloromethane-d_2): δ 1.63 (s, $^2J(^{195}\mathrm{Pt}-\mathrm{H}) = 87.8$ Hz, 6 H, Pt*Me*), 3.87 (s, 6 H, O*Me*), 7.01 ("d", $^3J(\mathrm{H^aH^b}) = 8.9$ Hz, 4 H, Ar H^a), 7.42 ("d", $^3J(\mathrm{H^aH^b}) = 8.9$ Hz, 4 H, Ar H^b), 9.30 (s, $^3J(^{195}\mathrm{Pt}-\mathrm{H}) = 28.7$ Hz, 2 H, NC*H*C*H*N). ^{13}C{^{1}H} NMR (75 MHz, dichloromethane-d_2): δ −11.5 ($^1J(^{195}\mathrm{Pt}-\mathrm{C}) = 806$ Hz, Pt*Me*), 56.0 (O*Me*), 114.4 (Ar C_m), 124.9 (Ar C_o), 143.6 (Ar C_{ipso}), 160.4 (Ar C_p), 160.8 (N*C*H*C*HN). UV−vis (acetonitrile): λ_{max} 394 (12.7), 564 (2.1), 595 (2.2). UV−vis (toluene): 411 (14.0), 605 (2.4), 649 (3.0). Anal. Calcd for $C_{18}H_{22}N_2O_2Pt$: C, 43.81; H, 4.49; N, 5.68; Pt, 39.53. Found: C, 44.32; H, 4.70; N, 6.43; Pt, 39.64.

(TolN=CMeCMe=NTol)PtMe$_2$ (1c): From $Pt_2Me_4(\mu\text{-}SMe_2)_2$ (500 mg, 0.870 mmol) and TolN=CMeCMe=NTol (460 mg, 1.740 mmol) in toluene (100 mL); dark purple shimmering microcrystals (716 mg, 84%). ^{1}H NMR (200 MHz, dichloromethane-d_2): δ 0.92 (s, $^2J(^{195}\mathrm{Pt}-\mathrm{H}) = 86.9$ Hz, 6 H, Pt*Me*), 1.43 (s, 6 H, NC*Me*C*Me*N), 2.43 (s, 6 H, Ar*Me*), 6.89 ("d", $^3J(\mathrm{H^aH^b}) = 8.3$ Hz, 4 H, Ar H^a), 7.29 ("d", $^3J(\mathrm{H^aH^b}) = 8.0$ Hz, 4 H, Ar H^b). ^{13}C{^{1}H} NMR (75 MHz, dichloromethane-d_2): δ −13.5 ($^1J(^{195}\mathrm{Pt}-\mathrm{C}) = 803$ Hz, Pt*Me*), 21.1 (NC*Me*C*Me*N), 21.1 (Ar*Me*), 122.0 (Ar C_o), 129.5 (Ar C_m), 136.2 (Ar C_p), 145.6 ($^2J(^{195}\mathrm{Pt}-\mathrm{C}) = 25.7$ Hz, Ar C_{ipso}), 171.2 ($^2J(^{195}\mathrm{Pt}-\mathrm{C}) = 16.7$ Hz, N*C*MeCMeN). UV−vis (acetonitrile): λ_{max} 372 (4.1), 510 sh (2.0), 541 (2.2). UV−vis (toluene): 453 (3.8), 595 (0.4). Anal. Calcd for $C_{20}H_{26}N_2Pt$: C, 49.07; H, 5.35; N, 5.72; Pt, 39.85. Found: C, 49.01; H, 5.29; N, 5.85; Pt, 40.03.

(AnN=CMeCMeAn)PtMe$_2$ (1d): from $Pt_2Me_4(\mu\text{-}SMe_2)_2$ (600 mg, 1.044 mmol) and AnN=CMeCMe=NAn (619 mg, 2.089 mmol) in toluene (130 mL); dark purple shimmering microcrystals (991 mg, 91%). ^{1}H NMR (300 MHz, dichloromethane-d_2): δ 0.95 (s, $^2J(^{195}\mathrm{Pt}-\mathrm{H}) = 86.6$ Hz, 6 H, Pt*Me*), 1.45 (s, 6 H, NC*Me*C*Me*N), 3.86 (s, 6 H, O*Me*), 6.95 ("d", $^3J(\mathrm{H^aH^b}) = 9.0$ Hz, 4 H, Ar H^a), 7.01 ("d", $^3J(\mathrm{H^aH^b}) = 9.0$ Hz, 4 H, Ar H^b). ^{13}C{^{1}H} NMR (75 MHz, dichloromethane-d_2): δ −13.5 ($^1J(^{195}\mathrm{Pt}-\mathrm{C}) = 801$ Hz, Pt*Me*), 21.1 (NC*Me*C*Me*N), 55.8 (O*Me*), 114.1 (Ar C_m), 123.4 (ArC_o), 141.3 ($^2J(\mathrm{Pt}-\mathrm{C}) = 26.0$ Hz, Ar C_{ipso}), 158.2 (Ar C_p), 171.4 ($^2J(\mathrm{Pt}-\mathrm{C}) = 18.2$ Hz, N*C*MeCMeN). UV−vis (acetonitrile): λ_{max} 369 (7.6), 510 sh (3.0), 543 (3.2). UV−vis (toluene): 378 (4.0), 550 (0.9), 597 (0.9). Anal. Calcd for $C_{20}H_{26}N_2O_2Pt$: C, 46.06; H, 5.03; N, 5.37; Pt, 37.41. Found: C, 46.58; H, 4.88; N, 5.76; Pt, 37.31.

[(TolN=CHCH=NTol)PtMe(NCMe)]$^+$(BF$_4^-$) (2a(BF$_4^-$)). A solution of **1a** (100 mg, 0.217 mmol) in acetonitrile (7 mL) was cooled to −13 °C, whereupon a 54% solution of HBF_4 in ether (31 μL, 0.23 mmol) was added with a syringe. The mixture was stirred for 2 h, while it was slowly warmed to ambient temperature. The solvent was removed, and the residue was washed with several portions of ether. The solid was dissolved in a minimum amount of dichloromethane. The product was obtained as an orange powder (89 mg, 72%) by the addition of pentane. ^{1}H NMR (200 MHz, dichloromethane-d_2): δ 1.08 (s, $^2J(^{195}\mathrm{Pt}-\mathrm{H}) = 76.6$ Hz, 3 H, Pt*Me*), 2.43 and 2.45 (s, 3 H each, Ar*Me*, Ar′*Me*), 2.44 (s, $^4J(^{195}\mathrm{Pt}-\mathrm{H}) = 13.9$ Hz, 3 H, PtNC*Me*), 7.18 ("d", $^3J(\mathrm{H^aH^b}) = 8.3$ Hz, 2 H, Ar H^a), 7.31 ("d", $^3J(\mathrm{H^aH^b}) = 8.4$ Hz, 2 H, Ar H^b), 7.38 ("d", $^3J(\mathrm{H^aH^b}) = 8.9$ Hz, 2 H, Ar′ H^a), 7.45 ("d", $^3J(\mathrm{H^aH^b}) = 8.8$ Hz, 2 H, Ar′ H^b), 8.94 (s, $^3J(^{195}\mathrm{Pt}-\mathrm{H}) = 99.8$ Hz, 1 H, NC*H*C′HN′), 8.98 (s, $^3J(^{195}\mathrm{Pt}-\mathrm{H}) = 35.6$ Hz, 1 H, NCHC′*H*N′). ^{13}C{^{1}H} NMR (75 MHz, acetonitrile-d_3): δ −10.8 ($^1J(^{195}\mathrm{Pt}-\mathrm{C}) = 674$ Hz, Pt*Me*), 21.1 and 21.3 (Ar*Me* and Ar′*Me*), 123.8 (s, Ar C_o), 123.8 ($^3J(^{195}\mathrm{Pt}-\mathrm{C} = 19.0$ Hz), Ar′ C_o), 130.5 and 131.2 (Ar C_m and Ar′ C_m), 141.0 and 142.8 (Ar C_p and Ar′ C_p), 145.2 and 145.8 (Ar C_{ipso} and Ar′ C_{ipso}), 162.5 ($^2J(^{195}\mathrm{Pt}-\mathrm{C}) = 57.0$ Hz, NC*H*C′HN), 173.5 (NCH*C*′HN). UV−vis (acetonitrile): λ_{max} 329 (6.9), 400 (9.9). Anal. Calcd for $C_{19}H_{22}BF_4N_3Pt$: C, 39.74; H, 3.86; N, 7.32. Found: C, 39.93; H, 3.86; N, 7.16.

[(AnN=CHCH=NAn)PtMe(NCMe)]$^+$(BF$_4^-$) (2b(BF$_4^-$)). A solution of **1b** (200 mg, 0.41 mmol) in acetonitrile (15 mL) was cooled to −13 °C, after which a 54% solution of HBF_4 in ether (60 μL, 0.44 mmol) was added with a syringe. The mixture was stirred for 2 h, while it was slowly warmed to ambient temperature. The solvent was removed, and the solid was washed with several portions of ether before it was dissolved in a minimum amount of acetonitrile. Precipitation by addition of toluene yielded the product as a red powder (222 mg, 90%). ^{1}H NMR (300 MHz, dichloromethane-d_2): δ 1.11 (s, $^2J(^{195}\mathrm{Pt}-\mathrm{H}) = 76.5$ Hz, 3 H, Pt*Me*), 2.46 (s, $^4J(^{195}\mathrm{Pt}-\mathrm{H}) = 14.0$ Hz, 3 H, PtNC*Me*), 3.87 and 3.91 (s, 3 H each, *Me*O, *Me*′O), 7.01 ("d", $^3J(\mathrm{H^aH^b}) = 9.0$ Hz, 2 H, Ar H^a), 7.10 ("d", $^3J(\mathrm{H^aH^b}) = 9.0$ Hz, 2 H, Ar H^b), 7.27 ("d", $^3J(\mathrm{H^aH^b}) = 9.0$ Hz, 2 H, Ar′ H^a), 7.56 ("d", $^3J(\mathrm{H^aH^b}) = 9.0$ Hz, 2 H, Ar′ H^b), 8.87 (s, $^3J(^{195}\mathrm{Pt}-\mathrm{H}) = 97.9$ Hz, 1 H, NC*H*C′HN′), 8.89 (s, $^3J(^{195}\mathrm{Pt}-\mathrm{H}) = 33.6$ Hz, 1 H, NC*H*C′HN′). ^{13}C{^{1}H} NMR (75 MHz, acetonitrile-d_3): δ −10.7 ($^1J(^{195}\mathrm{Pt}-\mathrm{C}) = 675$ Hz, Pt*Me*), 56.4 and 56.5 (O*Me* and O*Me*′), 115.0 and 115.9 (Ar C_m and Ar′ C_m), 125.6 ($^3J(^{195}\mathrm{Pt}-\mathrm{C}) = 20.4$ Hz, Ar′ C_o), 125.9 (Ar C_o), 140.9 and 141.4 (Ar C_{ipso} and Ar′ C_{ipso}), 161.5 and 163.0 (Ar C_p and Ar′ C_p), 160.7 ($^2J(^{195}\mathrm{Pt}-\mathrm{C}) = 56.8$ Hz, NCHC′HN) and 172.6 (N*C*MeC-′MeN) (for a complete assignment, see Table 4). UV−vis (acetonitrile): λ_{max} 322 (5.0), 432 (13.2). Anal. Calcd for $C_{19}H_{22}BF_4N_3O_2Pt$: C, 37.64; H, 3.66; N, 6.93. Found: C, 38.55; H, 3.75; N, 6.65.

[(TolN=CMeCMe=NTol)PtMe(NCMe)]$^+$(BF$_4^-$) (2c(BF$_4^-$). A solution of **1c** (150 mg, 0.31 mmol) in acetonitrile (14 mL) was cooled to −13 °C, whereupon a 54% solution of HBF_4 in ether (50 μL, 0.37 mmol) was added with a syringe. The mixture was stirred for 1.5 h, while it was slowly warmed to ambient temperature. Workup following the procedure for **2a**$^+$(BF$_4^-$) yielded the product as orange microcrystals (154 mg, 83%). ^{1}H NMR (200 MHz, dichloromethane-d_2): δ 0.62 (s, $^2J(^{195}\mathrm{Pt}-\mathrm{H}) = 75.1$ Hz, 3 H, Pt*Me*), 2.05 (s, $^4J(^{195}\mathrm{Pt}-\mathrm{H}) = 10.2$ Hz, 3 H, NC*Me*C′MeN), 2.11 (s, $^4J(^{195}\mathrm{Pt}-\mathrm{H}) = 13.6$ Hz, 3 H, PtNC*Me*), 2.13 (s, 3 H, NCMeC′*Me*N), 2.42 and 2.44 (s, 3 H each, Ar*Me* and Ar′*Me*), 6.92 ("d", $^3J(\mathrm{H^aH^b}) = 8.3$ Hz, 2 H, Ar H^a), 7.08 ("d", $^3J(\mathrm{H^aH^b}) = 8.3$ Hz, 2 H, Ar H^b), 7.33 ("d", $^3J(\mathrm{H^aH^b}) = 8.0$ Hz, 2 H, Ar′ H^a) and 7.37 ("d", $^3J(\mathrm{H^aH^b}) = 8.1$ Hz, 2 H, Ar′ H^b). ^{13}C{^{1}H} NMR (75 MHz, dichloromethane-d_2): δ −11.9 (Pt*Me*), 3.5 (PtNC*Me*), 19.9 and 21.6 (NC*Me*C-′*Me*N), 21.2 (Ar*Me* and Ar′*Me*), 121.9 and 122.3 (Ar C_o and Ar′ C_o), 130.2 (Ar C_m and Ar′ C_m), 138.6 and 138.7 (Ar C_p and Ar′ C_p), 142.7 and 143.1 (Ar C_{ipso} and Ar′ C_{ipso}), 173.8 and 183.7 (N*C*MeC′MeN). UV−vis (acetonitrile): λ_{max} 314 (4.8). Anal. Calcd for $C_{21}H_{26}BF_4N_3Pt$: C, 41.87; H, 4.35; N, 6.98. Found: C, 41.66; H, 4.27; N, 7.19.

[(AnN=CMeCMe=NAn)PtMe(NCMe)]$^+$(BF$_4^-$) (2d(BF$_4^-$)). A solution of **1d** (100 mg, 0.19 mmol) in acetonitrile (10 mL) was cooled to −13 °C, whereupon a 54% solution of HBF_4 in ether (26 μL, 0.19 mmol) was added with a syringe. The mixture was stirred for 1 h, while it was slowly warmed to ambient temperature. The product was obtained as orange crystals after recrystallization from acetonitrile/toluene (107 mg, 88%). ^{1}H NMR (200 MHz, dichloromethane-d_2): δ 0.65 (s, $^2J(^{195}\mathrm{Pt}-\mathrm{H}) = 75.1$ Hz, 3 H, Pt*Me*), 2.06 (s, $^4J(^{195}\mathrm{Pt}-\mathrm{H}) = 10.3$ Hz, 3 H, NC*Me*C′MeN), 2.15 (s, 3 H, NCMeC′*Me*N), 2.17 (s, $^4J(^{195}\mathrm{Pt}-\mathrm{H}) = 13.6$ Hz, 3 H, PtNC*Me*), 3.86 and 3.87 (s, 3 H each, O*Me* and O*Me*′), 6.97 ("d", $J(\mathrm{H^aH^b}) = 9.1$ Hz, 2 H, Ar H^a), 7.03, ("d", $J(\mathrm{H^aH^b}) = 9.1$ Hz, 2 H, Ar H^b) 7.08 ("d", $J(\mathrm{H^aH^b}) = 9.1$ Hz, 2 H, Ar′ H^a), 7.15 ("d", $J(\mathrm{H^aH^b}) = 9.1$ Hz, 2 H, Ar′ H^b). ^{13}C{^{1}H} NMR (75 MHz, dichloromethane-d_2): δ −11.7 (Pt*Me*), 3.6 (PtNC*Me*), 20.0 and 21.7 (NC*Me*C′*Me*N), 55.9 and 56.1 (O*Me* and O*Me*′), 114.8 and 114.8 (Ar C_m and Ar′ C_m), 123.8 and 123.8 (ArC_o and Ar′C_o), 138.2 and 138.7 (Ar C_{ipso} and Ar′ C_{ipso}), 159.4 and 159.8 (ArC_p and Ar′C_p), 173.6 and 183.9 (N*C*MeC′MeN). UV−vis (acetonitrile): λ_{max} 306 (4.4), 393 (5.1). Anal. Calcd for $C_{21}H_{26}BF_4N_3O_2Pt$: C, 39.76; H, 4.13; N, 6.62. Found: C, 40.55; H, 4.08; N, 7.32.

[(AnN=CHCH=NAn)PtMe$_3$(NCMe)]$^+$(OTf$^-$) (3b(OTf$^-$)). A solution of **1b** (150 mg, 0.30 mmol) in acetonitrile (15 mL) was cooled to −13 °C, whereupon methyl triflate (35 μL, 0.32 mmol) was added with a syringe. The mixture was stirred for 4 h, during which it was slowly warmed to ambient temperature. The solution was filtered, and the solvent was

Downloaded by CARLI CONSORTIUM on June 30, 2009
Published on August 6, 1998 on http://pubs.acs.org | doi: 10.1021/om9801498

removed. The yellow oily residue was washed repeatedly with ether, leading to the precipitation of red-orange crystals. Recrystallization from acetonitrile/toluene and drying in vacuo gave the product as orange crystals (189 mg, 89%). ^{1}H NMR (300 MHz, acetonitrile-d_3): δ 0.53 (s, $^2J(^{195}\mathrm{Pt}-\mathrm{H}) = 76.3$ Hz, 3H, PtMe_{ax}), 0.94 (s, $^2J(^{195}\mathrm{Pt}-\mathrm{H}) = 69.9$ Hz, 6 H, PtMe_{eq}), 3.87 (s, 6 H, O*Me*), 7.10 ("d", $^3J(\mathrm{H^aH^b}) = 9.0$ Hz, 4 H, Ar *H*^{a}), 7.30 ("d", $^3J(\mathrm{H^aH^b}) = 9.0$ Hz, 4 H, Ar *H*^{b}), 8.81 (s, $^3J(^{195}\mathrm{Pt}-\mathrm{H}) = 26.6$ Hz, 2 H, NC*H*C*H*N). ^{13}C{^{1}H} NMR (75 MHz, acetonitrile-d_3): δ −7.1 (PtMe_{ax}), −2.9 (PtMe_{eq}), 56.5 (O*Me*), 115.7 (Ar C_m), 125.3 (Ar C_o), 140.2 (Ar C_{ipso}), 162.0 (Ar C_p), 165.8 (NC*H*C*H*N). UV−vis (acetonitrile): λ_{max} 438 (12.4). Anal. Calcd for $C_{22}H_{28}F_3N_3O_5PtS$: C, 37.82; H, 4.04; N, 6.01; Pt, 27.92. Found: C, 37.98; H, 3.32; N, 6.52; Pt, 27.23.

Oxidation of 1b with $Cp_2Fe^+PF_6^-$ in Acetonitrile. Two NMR tubes equipped with ground-glass joints were each loaded with **1b** (5.4 mg, 0.011 mmol) and $Cp_2Fe^+PF_6^-$ (3.4 mg, 0.010 mmol). Acetonitrile-d_3 (0.7 mL) was added to each tube by vacuum transfer, and the tubes were sealed under vacuum. One tube was placed in a water bath at +55 °C. A rapid reaction ensued; the green suspension initially turned dark red and then, within $^1/_2$ min, changed to an orange-red transparent solution. The ^{1}H NMR spectrum showed the products to be **2b** (56%), **3b** (44%), and traces of methane. The composition remained constant for days at ambient temperature. The reaction in the second tube was started at −25 °C with a gradual temperature increase to ambient temperature over a period of 4 days. These conditions resulted in a very slow reaction, in which **2b** had not completely dissolved until the mixture was at ambient temperature. Nevertheless, the final product composition, as revealed by ^{1}H NMR, was essentially identical with that in the first tube (57% of **2b** and 43% of **3b**).

Constant-Potential Electrochemical Oxidation of 1b in Acetonitrile. All electrolysis experiments were performed in an H-shaped cell, the compartments of which were separated by a medium-frit glass junction. Gold- or platinum-gauze working electrodes were used. In the experiments, **1b** (10 mg, 0.020 mmol) was suspended in acetonitrile/0.05 M $Me_4N^+BF_4^-$ (20 mL) in the electrolysis cell. The solutions were electrolyzed at constant potentials until the current had dropped to less than 0.1 mA. The electrolyzed solutions were immediately transferred to round-bottomed flasks, and the solvent was removed. The residue was extracted with dichloromethane (leaving the electrolyte behind), and the extract was filtered. Dichloromethane was removed from the filtrate, and the residue was analyzed by ^{1}H NMR spectroscopy.

(a) Electrolysis at *E* = 0.95 V vs Fc, Au Working Electrode, 1.6 faraday/mol of Charge. The ^{1}H NMR spectrum showed **2b** (20%), **3b** (18%), *cis*,*cis*-[(AnN=CHCH=NAn)PtMe_2(NCMe)$_2$]$^{2+}$ (**4b**, 53%), and *cis*,*trans*-[(AnN=CHCH=NAn)PtMe_2(NCMe)$_2$]$^{2+}$ (**5b**, 9%). ^{1}H NMR of **4b** (300 MHz, acetonitrile-d_3): δ 1.59 (s, $^2J(^{195}\mathrm{Pt}-\mathrm{H}) = 71.4$ Hz, 3 H, Pt*Me*), 1.61 (s, $^2J(^{195}\mathrm{Pt}-\mathrm{H}) = 61.2$ Hz, 3 H, Pt*Me*), 2.61 (s, $^4J(^{195}\mathrm{Pt}-\mathrm{H}) = 10.9$ Hz, 3 H, PtNC*Me*), 2.62 (s, $^4J(^{195}\mathrm{Pt}-\mathrm{H}) = 12.4$ Hz, 3 H, PtNC*Me*), 3.88 (s, 3 H, *Me*O), 3.93 (s, 3 H, *Me*O), 7.12 ("d", $J(\mathrm{H^aH^b}) = 9.0$ Hz, 2 H, Ar H^a), 7.21 ("d", $J(\mathrm{H^aH^b}) = 9.1$ Hz, 2 H, Ar H^b), 7.29 ("d", $J(\mathrm{H^aH^b}) = 9.2$ Hz, 2 H, Ar′ H^a), 7.63 ("d", $J(\mathrm{H^aH^b}) = 9.1$ Hz, 2 H, Ar′ H^b), 8.75 (d, $^3J(\mathrm{H}-\mathrm{H}) = 1.0$ Hz, $^3J(^{195}\mathrm{Pt}-\mathrm{H}) = 94.4$ Hz, 1 H, NC*H*CHN), 8.85 (d, $^3J(\mathrm{H}-\mathrm{H}) = 1.0$ Hz, $^3J(^{195}\mathrm{Pt}-\mathrm{H}) = 30.4$ Hz, 1 H, NCHC′*H*N). ^{1}H NMR of **5b** (300 MHz, dichloromethane-d_2): δ 2.66 (s, $^4J(^{195}\mathrm{Pt}-\mathrm{H}) = 10.1$ Hz, 6 H, PtNC*Me*). ^{1}H NMR of **5b** (300 MHz, acetonitrile-d_3): δ 1.85 (s, $^2J(^{195}\mathrm{Pt}-\mathrm{H}) = 62.7$ Hz, 6 H, Pt*Me*), 3.89 (s, 6 H, *Me*O), 7.16 ("d", $J(\mathrm{H^aH^b}) = 9.1$ Hz, 4 H, Ar *H*^{a}), 7.39 ("d", $J(\mathrm{H^aH^b}) = 9.1$ Hz, 4 H, Ar *H*^{b}), 9.05 (s, $^3J(^{195}\mathrm{Pt}-\mathrm{H}) = 25.6$ Hz, 2 H, NC*H*C*H*N).

(b) *E* = 0.85 V, Au Working Electrode. The solution was electrolyzed for 3930 s, at which point 1.31 faraday/mol had been transferred. ^{1}H NMR showed a product composition consisting of **2b** (33%), **3b** (32%), **4b** (26%), and **5b** (8%).

(c) *E* = 0.95 V, Pt Working Electrode. The solution was electrolyzed for 3000 s, at which point 1.21 faraday/mol had been transferred. ^{1}H NMR showed a product composition consisting of **2b** (35%), **3b** (31%), **4b** (28%), and **5b** (6%).

(d) *E* = 0.85 V, Pt Working Electrode. The solution was electrolyzed for 4500 s, at which point 1.07 faraday/mol had been transferred. However, at this point a considerable current (>0.1 mA) still flowed. ^{1}H NMR showed a product composition consisting of **2b** (50%) and **3b** (50%).

Attempted Preparation of Salts of [(AnN=CHCH=NAn)PtMe_2(NCMe)$_2$]$^{2+}$ (4b and 5b). An NMR tube equipped with a ground-glass joint was loaded with **2b**(BF_4^-) (3.0 mg, 4.9 μmol) and MeOTf (0.6 μL, 5 μmol). Acetonitrile-d_3 (0.7 mL) was added by vacuum transfer, and the tube was sealed under vacuum. ^{1}H NMR analysis of the sample showed no reaction at ambient temperature. When the tube was slowly heated to 75 °C, **2b** was completely consumed to give only uncharacterizable products. No traces of **4b** or **5b** were observed.

X-ray Crystallographic Structure Determination of 1b and 3b(OTf$^-$). Crystals of **1b** and **3b**(OTf$^-$) were obtained by crystallization from dichloromethane and acetonitrile/toluene, respectively. X-ray data were collected on a Siemens SMART CCD diffractometer[34] using graphite-monochromated Mo *K*α radiation. Data collection method: ω-scan, range 0.6°, crystal to detector distance 5 cm; further information given in Table 2. Data reduction and cell determination were carried out with the SAINT and XPREP programs.[34] Absorption corrections were applied by the use of the SADABS program.[35]

The structures were determined and refined using the SHELXTL program package.[36] The non-hydrogen atoms were refined with anisotropic thermal parameters; hydrogen positions were calculated from geometrical criteria with isotropic thermal parameters. Final figures of merit are included in Table 2.

Positional and equivalent isotropic thermal parameters for non-hydrogen atoms for **1b** and **3b**(OTf$^-$) are listed in Table 3. Lists of thermal parameters, hydrogen parameters, and all bond lengths, bond angles, and torsion angles may be obtained as Supporting Information.

Acknowledgment. We gratefully acknowledge generous support from the Norwegian Research Council, NFR (stipends to L.J. and C.R.), and from Statoil under the VISTA program, administered by the Norwegian Academy of Science and Letters.

Supporting Information Available: Tables and figures giving details of the full NMR characterization of **2b** and tables of thermal parameters, hydrogen parameters, and all bond lengths, bond angles, and torsion angles and figures giving additional views of **1b** and **3b**(OTf$^-$) (22 pages). Ordering information is given on any current masthead page.

OM9801498

(34) SMART and SAINT Area-detector Control and Integration Software; Siemens Analytical X-ray Instruments Inc., Madison, WI.
(35) Sheldrick, G. M. Private communication, 1996.
(36) Sheldrick, G. M. SHELXTL, Version 5; Siemens Analytical X-ray Instruments Inc., Madison, WI.